Evaluating the Electromagnetic Shielding of Continuous Carbon Fiber Parts Produced by Additive Manufacturing

Luís C. Martins , Cátia S. Silva , Leandro C. Fernandes , Álvaro M. Sampaio , António J. Pontes *

Posted Date: 12 October 2023

doi: 10.20944/preprints202310.0758.v1

Keywords: additive manufacturing; material extrusion; continuous fiber reinforcement; electromagnetic shielding effectiveness; thermoplastic composite; continuous carbon fiber; multi-material

Article

Evaluating the Electromagnetic Shielding of Continuous Carbon Fiber Parts Produced by Additive Manufacturing

Luís C. Martins [1], Cátia S. Silva [1,2], Leandro C. Fernandes [1,2], Álvaro M. Sampaio [2,3] and António J. Pontes [1,2,*]

[1] Institute of Polymers and Composites, Department of Polymer Engineering, Campus de Azurém, University of Minho, 4800-058 Guimarães, Portugal
[2] DONE Lab – Advanced Manufacturing of Polymers and Tools, Campus de Azurém, University of Minho, 4800-058 Guimarães, Portugal
[3] Lab2PT, School of Architecture, Campus de Azurém, University of Minho, 4800-058 Guimarães, Portugal
* Correspondence: pontes@dep.uminho.pt.

Abstract: Electronic devices are sensitive to electromagnetic (EM) emissions requiring electromagnetic shielding protection to assure good operation, preventing noise, malfunctioning, or even burning. To assure protection, it is important to develop suitable material and design solutions for electronic enclosures. Most common enclosures are made with metal alloys by traditional manufacturing methods. However, resourcing to thermoplastic composites combined with additive manufacturing (AM) technologies emerges as an alternative that enables to fabricate complex parts that are lightweight, consolidated and oxidation and corrosion resistant. In this research, an AM technique based in material extrusion was used to print 2 mm thick specimens with a multi-material made of micro-carbon fiber (CF) filled polyamide, reinforced, at specific layers, by continuous carbon fibers stacked with a 90° rotation to each other. Specimens electromagnetic shielding effectiveness (EMSE) was evaluated in the frequency band of 0.03 – 3 GHz by coaxial transmission line method. Depending on the number of CF layers, the EM shielding obtained can up to 70 dB, with a specific shielding up to 60 dB.cm^3/g, predominantly by absorption mechanism, being 22 times higher that without the CF layers. These findings fundament this innovative approach for lightweight customizable solutions for EM shielding applications.

Keywords: additive manufacturing; material extrusion; continuous fiber reinforcement; electromagnetic shielding effectiveness; thermoplastic composite; continuous carbon fiber; multi-material

1. Introduction

Nowadays there are many electronic devices for various applications using a variety of frequency bands such as wireless LAN (2–6 GHz), Bluetooth (2.4 GHz), mobile phones (0.8–3 GHz), and military communication/radar (8–12 GHz) [1]. These devices, when in operation, emit electromagnetic (EM) fields and are susceptible to electromagnetic interference (EMI) originated from the surrounding devices or from natural sources. Therefore, all electronics must be enclosed by an electromagnetic impermeable material (shield) which provides mechanical support and prevents signal interference or electrostatic discharge (ESD) which can lead to noise, malfunction, or even burning [2,3]. The efficiency of a barrier, also known as EMI shielding effectiveness (SE), is an EM field ratio between the source and the receptor that can quantify the attenuation of the wave's propagation through the material or apertures of an enclosure, and is achieved through three different loss mechanisms, namely reflection, absorption, and multiple reflections [2–6]. SE is expressed in decibel (dB), and the common requirement for commercial electronics is the range from 40 to 60 dB [7], though an SE of 30 dB (99.9% attenuation) is also considered an adequate level of shielding for many applications [8,9].

 doi:10.20944/preprints202310.0758.v1

SE is directly proportional to the material electrical conductivity and that is the reason why conducting metal alloys, such as, aluminum, copper, steel or silver are broadly used as reflecting EMI shielding materials. However, the high density, poor mechanical flexibility, low resistance to chemicals, low resistance to oxidation and high reflectance constricts the use of these metallic alloys. Because of these reasons, metallic shields are being replaced by flexible hybrid shields made by metamaterials [10,11], intrinsically conducting polymers [12–14] or thermoplastic composites [9,15–17].

The use of thermoplastics composites reinforced with carbon allotropes, such as, carbon nanotubes (CNT), carbon black (CB), carbon fibers (CF) or graphene (Gr) is very appealing for EMI shielding [13,18,19]. The low density, easy processability and resistance to corrosion and oxidation of these materials allows many improvements over traditional conductive materials, as more complex, flexible and lightweight enclosures, can be fabricated as a sole part which reduces or eliminates seams, preventing EM radiation leakage and SE dropping [4,6,20].

Thermoplastic composites have been explored more intensively by conventional fabrication techniques, such as, compression molding or injection molding [21–28]. However, recently, additive manufacturing (AM) technologies improved significantly and are becoming more adopted to manufacture final products. AM is a competitive digital manufacturing process that allows to fabricate complex and functional geometries, due to the inherent design freedom that the layer-by-layer process enables. In combination with design exploration methods, such as, generative design and topology optimization, AM can overcome the traditional manufacturing limits and achieve a more efficient product performance while improving manufacturability, by reducing lead time, cost and material consuming [29,30]. AM processes are commonly divided according to seven categories, namely: (i) binder jetting; (ii) direct energy deposition; (iii) material extrusion; (iv) VAT polymerization; (v) material jetting; (vi) sheet lamination; and (vii) laminated object manufacturing (LOM) [31]. Focusing on the material extrusion (ME) technology, it consists of a bottom-up process based on the extrusion of material in the filament form onto a build platform in a layer-by-layer process, where the filament is deposited on top of the subsequent deposited layer until the part to be produced is complete. At the end of the deposition, the filament solidifies [32]. The main benefits of the ME process include the ease and relative speed to produce functional products at a competitive cost, and also the large range of materials commercially available and the possibility to develop a customizable material adjusted to the product requirements [32,33]. Regarding the part quality and mechanical properties, these are dependent on process parameters, such as, build orientation, layer thickness, layer adhesion, type of infill, air gap, raster angle and raster width [32,34].

AM, specifically the ME technology, has been used in the development of plastic composite parts with electrical conductivity properties and EM shielding characteristics. Most of the studies report the optimization of the printing process and the manipulation of filament properties by adding conductive fillers, in order to improve the required property, either mechanical, electrical, thermal or electromagnetic [26,35–42]. For example, the addition of CNT as a conductive nano-filler to the polymer filament, or a hybrid combination with one additional filler, such as CB, was developed to improve the electrical conductivity and/or electromagnetic shielding properties of the products printed by ME. Dorigato et al. [36] developed a multi-walled carbon nanotubes (MWCNT) filled acrylonitrile-butadiene-styrene (ABS) compound showing that the MWCNT improved the tensile, electrical and thermal properties. Furthermore, they also report that these properties are also dependent on the printing orientation. Chizari et al. [26] used the ME process to produce conductive microstructures for the functional optimization of lightweight and semi-transparent EMI shields. They formulated a highly conductive carbon nanotubes/polylactic acid (CNT/PLA) printable ink to fabricate 3D scaffolds with significant improvement to the specific EMSE relatively to CNT/PLA hot-pressed in solid forms (~70 vs ~37 $dB.cm^3/g$). Schmitz et al. [37,41] fabricated samples via ME with an ABS filled with CNT, CB or a hybrid combination (CNT/CB). They reported that the electrical conductivity, EMSE and mechanical properties of printed parts were considerably dependent on the printing orientation. The EM shielding and respective electrical conductivity were more efficiently improved with the increase of CNT rather than increasing the CB amount. Furthermore, the EMSE

 doi:10.20944/preprints202310.0758.v1

increased with the increase layer thickness and showed an anisotropic behavior when printed in the perpendicular orientation. Wang et al. [43] produced 3D-printing scaffold structures with carbon nanotube/polylactic acid composite. The highly conductive CNTs coated on the 3D-printed PLA scaffolds increased the interconnected networks after compression molding which translated to an enhanced EMI shielding performance as high as 67 dB, while also improving the mechanical robustness of 3D-CNT/PLA. The use of AM methods with graphene-based polymer composites has been indicated as very promising for the enhancement of material properties to enable novel applications in fields like biomedicine, energy, sensing, and electromagnetic interference shielding [39].

Additive manufacturing can also be used to develop advanced materials as described by Fan et al. [10] and by Lee et al. [42]. By designing complex structures and arranging the distribution of materials with different physical parameters, AM technology provides a direct and efficient way to develop metamaterials with electromagnetic absorption properties [10]. Under the ME printing process of a graphene-polyamide-6 composite filament, it was demonstrated that the introduction of internal geometric assemblies significantly improved EMSE [42]. Moreover, the ME technology was used by Duan et al. [44] to fabricate gradient composite metastructures to effectively absorb microwave signals demonstrating that the designed metastructure with the thickness of 10 mm can achieve the 10 dB absorbing bandwidth in the frequency range from 5 to 40 GHz.

Recent advances allowed the development of products by a multi-material AM fabrication process of continuous fiber reinforced polymer composites, with increased performance relatively to conventional short fiber filled filaments. Parmiggiani et al. [45] studied the mechanical resistance of components made with continuous carbon fiber (CCF) reinforced thermoplastic materials fabricated by ME focusing on the influence of the fiber orientation (0°, 45°, and 90°) on the tensile and flexural properties of the produced parts. [45] Blok et al. [46] also used the ME technology from Markforged, Inc to study the print capability of CCF for further understanding the advantages and limitations of this printing process, in comparison to the printing of chopped short-CF filled polyamide filament. The tensile strength and stiffness of the CCF printed parts were more than an order of magnitude higher than the short fiber reinforced polyamide printed parts.

Current technology advances in AM highlight the fabrication of low cost, and high-efficient complex structures with electromagnetic shielding characteristics. However, at the time of writing, the authors are not aware of the existence of peer studies that encompasses the use of ME technology to print CCF reinforced materials to develop a functional enclosure for EMI shield. Hence the relevance of sharing the findings of this study with the scientific and engineering community. This paper presents a study regarding the evaluation of the electromagnetic shielding performance obtained by specimens manufactured by continuous fiber reinforcement considering process parameters variation and specimen thickness.

2. Materials and Methods

2.1. Materials

The materials used for the production of the specimens were supplied by *Markforged, Inc*. The polymeric filament consisted on a chopped micro-CF reinforced Nylon composite, with trade name *Onyx*™. Main properties include a tensile modulus of 2.4 GPa, a tensile train and break of 25%, a flexural strength of 71 MPa, a flexural modulus of 3 GPa, a heat deflection temperature of 145°C and, a density of 1.2g/cm^3. Regarding the reinforcement material, a continuous CF filament was selected that presents a tensile modulus of 60 GPa, a tensile train and break of 1.5%, a flexural strength of 540 MPa, a flexural modulus of 51 GPa, a heat deflection temperature of 105°C and, a density of 1.4g/cm^3 [47].

2.2. Production

The Material Extrusion (ME) technology was used to produce two types of specimens, as shown in Figure 1 (a). The load specimen consists of a flat solid disk with six peripheral holes for fixation on

Preprints (www.preprints.org) | NOT PEER-REVIEWED | Posted: 12 October 2023 doi:10.20944/preprints202310.0758.v1

the apparatus and is used for EMSE evaluation while, the reference specimen has a toroid shape section removed near the center of the specimen and is used to create a baseline for the EMSE analysis. Both flat disk specimens are built of the same material and have the same diameter of 60 mm and thickness of 2 mm, which is a common thickness for plastic parts. The specimens were produced resourcing to the continuous fiber reinforcement (CFR) process from *Markforged* with the equipment *Mark Two*™. Both specimens were built with the positioning shown in Figure 1 (b).

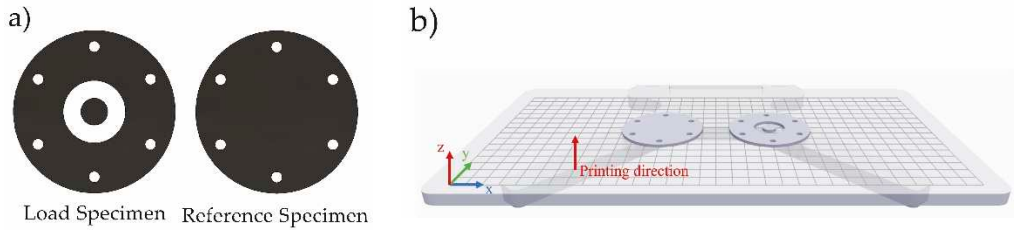

Figure 1. (a) CAD representation of the printed load; (b) CAD representation of the reference specimens; and (c) build platform depicting with specimens positioning for manufacturing, image from software *Eiger™ 3D Printing Software* from *Markforged*.

The printing process considered a layer heigh of 0.125 mm, a solid fill pattern (fill density of 100%) and two Onyx (O) peripheral wall layers (0.8 mm). The 2 mm thick specimens were printed in an isotropic pattern with an alignment angle of -45° or 45°, as shown in Figure 2, which were alternated between layers up to a total number of 16 layers. Such customization was carried according to the specifications permitted by the *Markforged cloud software, Eiger*™.

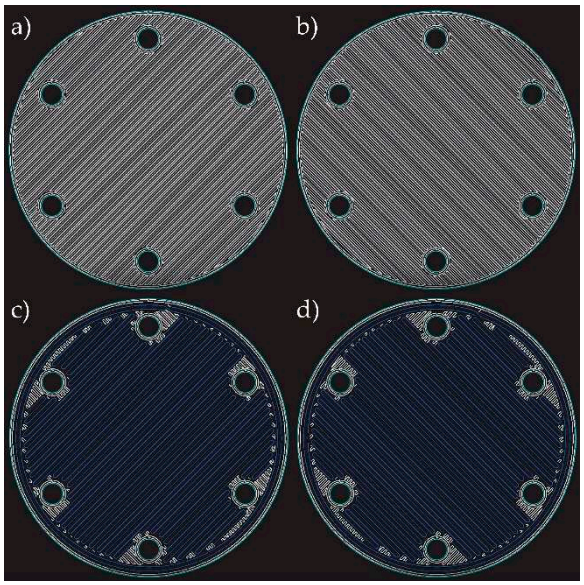

Figure 2. Printing patterns, established by the *Eiger™ 3D Printing Software*, for Onyx™ (white) and carbon fiber (blue): *Onyx*™ with (a) -45° pattern; (b) 45° pattern; and CF with (c) -45° pattern; and (d) 45° pattern.

In this research, a total of 9 type of specimens were printed. One specimen was printed totally with *Onyx*™, while the remaining specimens were reinforced with continuous carbon fibers in some of the sliced layers of the sample. Since the *Eiger™ 3D Printing Software* locks the first (layer 1) and last layer (layer 16) to be printed with Onyx™, the others 14 layers were used for CF insertion. As previously stated, the CF and *Onyx*™ were printed in an isotropic pattern with an alignment angle of -45° or 45°, which was alternated in each layer. This process was used to produce composite samples with just 1 CF layer up to 14 layers, as shown in Table 1 and Table 2.

Table 1. Design layout for the produced specimens. O is Onyx™ and CF is carbon fiber.

Preprints (www.preprints.org) | NOT PEER-REVIEWED | Posted: 12 October 2023 doi:10.20944/preprints202310.0758.v1

Layers	Designation of specimens (*O - Onyx™; CF is carbon fiber*)								
	0 CF	**1 CF**	**2 CF**	**4 CF**	**6 CF**	**8 CF**	**10 CF**	**12 CF**	**14CF**
16	O 45°	O 45°	O 45°	O 45°	O 45°	O 45°	O 45°	O 45°	O 45°
15	O -45°	O -45°	O -45°	O -45°	O -45°	O -45°	O -45°	O -45°	CF -45°
14	O 45°	O 45°	O 45°	O 45°	O 45°	O 45°	O 45°	CF 45°	CF 45°
13	O -45°	O -45°	O -45°	O -45°	O -45°	O -45°	CF -45°	CF -45°	CF -45°
12	O 45°	O 45°	O 45°	O 45°	O 45°	CF 45°	CF 45°	CF 45°	CF 45°
11	O -45°	O -45°	O -45°	O -45°	CF -45°	CF -45°	CF -45°	CF -45°	CF -45°
10	O 45°	O 45°	O 45°	CF 45°	CF 45°	CF 45°	CF 45°	CF 45°	CF 45°
9	O -45°	CF -45°	CF -45°	CF -45°	CF -45°	CF -45°	CF -45°	CF -45°	CF -45°
8	O 45°	O 45°	CF 45°	CF 45°	CF 45°	CF 45°	CF 45°	CF 45°	CF 45°
7	O -45°	O -45°	O -45°	CF -45°	CF -45°	CF -45°	CF -45°	CF -45°	CF -45°
6	O 45°	O 45°	O 45°	O 45°	CF 45°	CF 45°	CF 45°	CF 45°	CF 45°
5	O -45°	O -45°	O -45°	O -45°	O -45°	CF -45°	CF -45°	CF -45°	CF -45°
4	O 45°	O 45°	O 45°	O 45°	O 45°	O 45°	CF 45°	CF 45°	CF 45°
3	O -45°	O -45°	O -45°	O -45°	O -45°	O -45°	O -45°	CF -45°	CF -45°
2	O 45°	O 45°	O 45°	O 45°	O 45°	O 45°	O 45°	O 45°	CF 45°
1	O -45°	O -45°	O -45°	O -45°	O -45°	O -45°	O -45°	O -45°	O -45°

Some theoretical characteristics for the load specimens printing design were provided by *Markforged Eiger™ 3D Printing Software* and are exhibited in Table 2 and Figure 3. In Figure 3 it is possible to verify the CF volumes (in blue) inside the specimen's preview model. The *Onyx*™ baseline specimen (corresponding to 0CF) highlights the absence of CF as there are no blue outlines. In Table 2, the "print time", "*Onyx*™ volume", "CF volume" and "part mass" characteristics are theoretical estimation provided by the software, while the "part density" is an arithmetic division between the "part mass" and the sum of the constituent's volumes. Additionally, Figure 3 shows a photo of each produced specimen. Since the base and top layers are both printed in *Onyx*™, the appearance of the samples is identical.

Table 2. Load specimens' characteristics.

Layers	Designation of specimens (*O - Onyx™; CF is carbon fiber*)								
	0 CF	**1 CF**	**2 CF**	**4 CF**	**6 CF**	**8 CF**	**10 CF**	**12 CF**	**14CF**
Print time (min)	51	57	60	64	67	75	80	84	85
CF ∑ layer (mm)	0	0.125	0.25	0.5	0.75	1	1.25	1.5	1.75
Onyx™ (cm^3)	5.39	5.41	5.14	4.57	4.01	3.43	2.85	2.27	1.68
CF volume (cm^3)	0	0.25	0.56	1.12	1.68	2.24	2.79	3.35	3.91
Part mass (g)	6.36	6.46	6.51	6.61	6.71	6.8	6.89	6.97	7.05
Part density (g/cm^3)	1.18	1.14	1.14	1.16	1.18	1.20	1.22	1.24	1.26

Preprints (www.preprints.org) | NOT PEER-REVIEWED | Posted: 12 October 2023 doi:10.20944/preprints202310.0758.v1

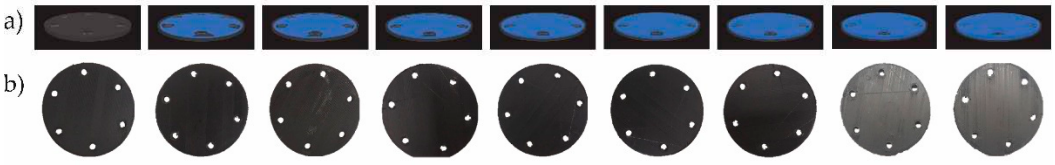

Figure 3. (a) Eiger™ model and; (b) photographic registry of each specimen from left to right: 0 CF, 1CF, 2CF, 4CF, 6CF, 8CF, 10CF, 12 CF and 14CF, respectively.

2.3. Characterization

This section presents the characterization procedure defined for the specimens produced, which includes an evaluation of the quality of the specimens and an electrical evaluation based on the electromagnetic shielding effectiveness and electrical resistivity.

2.3.1. Thickness, weight and density

Specimens' density was measured following to Archimedes principle. According to this principle, the volume of an immersed body is equal to the volume of the displaced volume. Therefore, a body immersed in a liquid is subjected to a buoyancy force equal to the weight of the liquid displaced by the volume of the body. The specific density is calculated using the equation:

$$\rho = \frac{W_{body,air} \times \rho_{liquid}}{W_{body,air} - W_{body,liquid}}, \quad (1)$$

where $W_{body,air}$ is the weight of the body in air, $W_{body,liquid}$ is the weight of the body in the liquid and, ρ_{liquid} is the specific density of the liquid.

The procedure for the density measure was performed with an analytical balance AS 202.R2 from *Radwag* with SDK 01 density kit from *Scaltec Lda*.

Regarding the measurement of the specimens' thickness, a *Mitutoyo Digimatic Caliper* was used.

2.3.2. Morphology

The morphology of the printed specimens was observed along the thickness cross-section with a *Leica DMS1000* digital microscope using a magnification of 6 times.

2.3.3. Electromagnetic shielding effectiveness

EMSE measurements were performed with a test procedure that follows the ASTM D4935-99 Standard (Standard Test Method for Measuring the Electromagnetic Shielding Effectiveness of Planar Materials) [48] wherein the sample is placed between two coaxial flanges which acts both as sample holder and transverse electromagnetic (TEM) waveguide, as used by Hong et al. [49], Sarto & Tamburrano [50] and Vasquez et al. [51]. The sample holder is an enlarged coaxial transmission line, made in a Brass alloy designed to support 60 mm diameter samples maintaining a characteristic impedance of 50 Ω throughout the entire length of the holder, and it is connected to a Vector Network Analyzer (VNA) (R&S®ZVL3) with the assistance of two coaxial cables and two 10 dB 50 Ω attenuators. Figure 4 depicts the testing apparatus.

Preprints (www.preprints.org) | NOT PEER-REVIEWED | Posted: 12 October 2023 doi:10.20944/preprints202310.0758.v1

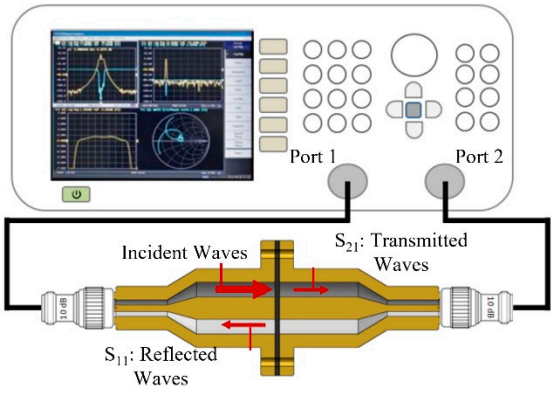

Figure 4. Shielding apparatus schematic representation.

Shielding Effectiveness (SE) was measured at the frequency range between 30 MHz and 3 GHz, which is a radio frequency spectrum common to automotive standards for electromagnetic compatibility (CISPR 25) [52], and is the VNA limit range. The VNA used an input power of 0 dBm, corresponding to 1 mW, to generate EM waves and recorded the scattering parameters S11 (reflection) and S21 (transmission) to determine the total EMSE and the respective shielding components according to the following equation [41,42,53–55]:

$$SE_T(dB) = SE_R + SE_A + SE_M, \quad (2)$$

where, SE_R is the shielding by reflection, SE_A is the shielding by absorption and, SE_M is the shielding by multiple reflections. SE_R and SE_A were calculated using the following equations:

$$SE_R(dB) = -10\log_{10}(1 - R), \quad (3)$$

$$SE_A(dB) = -10\log_{10}\left(\frac{T}{1 - R}\right), \quad (4)$$

wherein the reflected coefficient (R) and transmission coefficient (T) were directly obtained as:

$$R = |S_{11}|^2, \quad (5)$$

$$T = |S_{21}|^2, \quad (6)$$

Since the microwave multiple internal reflections (SE_M) can be negligible when SE_T is higher than 10 dB [54] the total shielding was calculated as:

$$SE_T(dB) = SE_R + SE_A, \quad (7)$$

2.3.4. Electrical resistivity

The electric resistivity of the filaments was measured according to the Ohms law using a four-point probe method using the *Keithley 2635B System SourceMeter* and *Keithley 5809* clips according to the equation:

$$\rho(\Omega.cm) = \frac{V \times A}{l \times I}, \quad (8)$$

where V is the applied voltage, A is the area of the filament cross-section, I is the reading current and l if the distance between the clip electrodes.

For the printed specimens, the electrical resistivity was measured according to the ASTM D257 standard "Standard Methods of Test for Electrical Resistance of Insulation Materials" by using the *Keithley 2635B System SourceMeter* and the *Keithley 8009* resistivity test fixture and was calculated with the equation:

 doi:10.20944/preprints202310.0758.v1

$$\rho(\Omega.cm) = \frac{22{,}9 \times V}{t \times I}, \quad (7)$$

where V is the applied voltage, t is the average thickness of the specimen, and I is the reading current.

3. Results and discussion

This section presents the results and respective discussion and it is divided in two main points. In the first point it is presented a discussion of some aspects related to the quality of the produced specimens, in particular, the measured thickness, weight, and density, in comparison to the estimations provided by the software *Eiger*™. A morphologic evaluation is also shown in relation to the weight and density of the composite specimens. In the second point, the results and discussion of the most important aspect of the research, the electromagnetic shielding of the printed composites, is presented as a function of the of the number of continuous CF layers is presented. Lastly, a brief comparison regarding the performance of these material in comparison with materials in the same property category is presented.

3.1. Quality of the printed composite specimens

The thickness, weight and density were measured on all specimens to verify the physical differences obtained from the respective printing process. It is known that these characteristics influence the total EM shielding, so their management is important for quality and performance control [9,26,56]. The respective measured values are shown in Table 3, and a comparative analysis with the theoretical values from the software are shown in Figure 5.

Table 3. Specimens' average physical dimensions.

ID	0 CF	1 CF	2 CF	4 CF	6 CF	8 CF	10 CF	12 CF	14CF
Thickness (mm)	1.99	2.00	2.01	2.01	2.00	2.02	2.03	2.03	2.03
Weight (g)	5.994	6.131	6.228	6.232	6.308	6.351	6.384	6.403	6.455
Density (g/cm^3)	1.142	1.137	1.161	1.135	1.134	1.123	1.121	1.106	1.150

Regarding the specimens' thickness, measurements were similar for all samples, and near the nominal thickness of 2 mm. Therefore, one can affirm that any variation to the shielding performance is derived from the composite content (i.e., *Onyx*™ and/or CF layers) and internal morphology along the part thickness.

As for the weight of the specimens, it was noticed (as shown in Figure 5 (a)) that the measured values are all bellow the expected values indicated by the software, by near 6% on average. The lowest weight of specimens is a result of lower real density. The experimental test indicates that the actual density values are lower than those estimated by approximately 4.6%, on average. This variation is an effect induced by the porosity inside the specimen, in particular, voids between layers which is verified by microscopic analysis shown in Figure 6. This effect was also observed in the research made by Blok (2018) [46]. Furthermore, the density difference to nominal values is higher for the specimens with higher CF layers, especially for the specimens with 8, 10 and 12 layers of CF where the presence of voids is more evident.

Preprints (www.preprints.org) | NOT PEER-REVIEWED | Posted: 12 October 2023 doi:10.20944/preprints202310.0758.v1

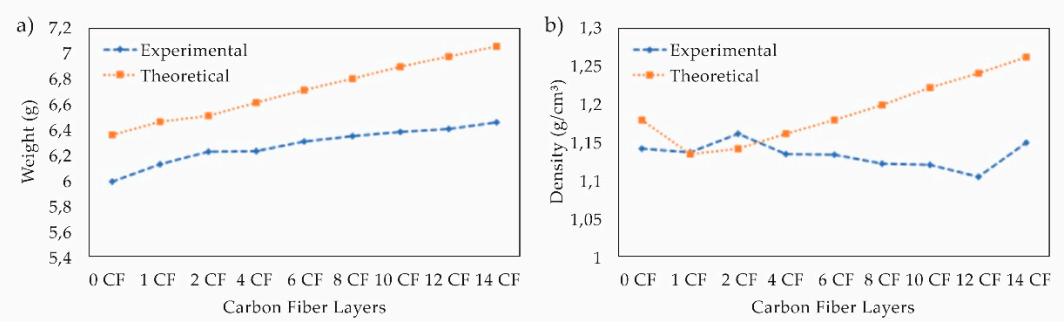

Figure 5. Experimental and theoretical values for: (a) part weight; and (b) part density.

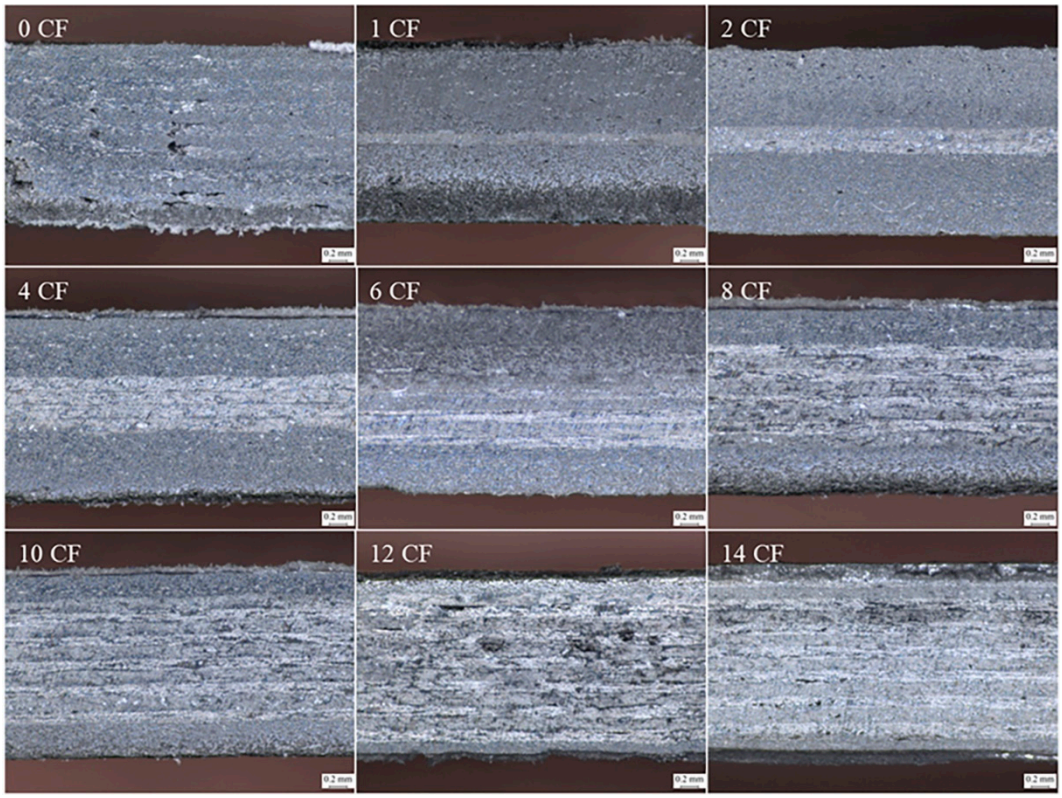

Figure 6. Microscopy of specimens' cross-section.

3.2. Electromagnetic shielding

In this topic is presented the results and discussion of the evaluation of the electromagnetic shielding. Since sample density can influence the EM shielding [26,56], a normalization to the different density values was performed, referred as specific SE, and is presented in the discussion bellow.

Focusing on the EM shielding analysis, it is possible to observe by the average total shielding, shown in Figure 7, evidence of a high improvement of shielding performance with the printing of the continuous CF layers on the internal layers of the composite specimen, from less than 10 dB (0 CF) up to 70 dB (14 CF). This enhancement is higher when a combination of at least 2 CF layers is used, as noted by the SE jump from 1 CF layer to 2 CF layers. The two layers tied together create an overlap of the CF printed pattern thicker, which reduce the voids between the CF deposited filaments in the same layer.

Above two CF layers it is possible to verify that the EMSE follows a linear proportionality with the increase of two combined CF layers. This behavior is highlighted in Figure 7 (b) and the coefficient

Preprints (www.preprints.org) | NOT PEER-REVIEWED | Posted: 12 October 2023 doi:10.20944/preprints202310.0758.v1

of linearity varies with the frequency. However, on average, the EMSE increases approximately 4 dB with the increase of a combination of two CF layers.

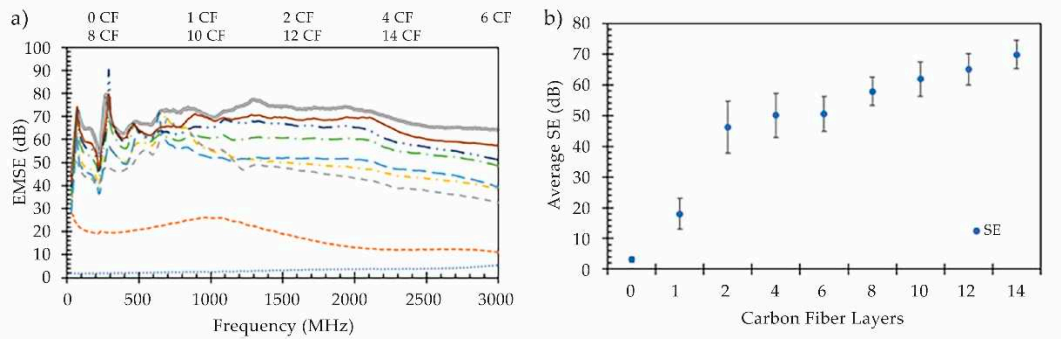

Figure 7. EMSE results: (a) EMSE for all specimens as function of frequency; and b) average EMSE as function of the number of CF layers.

Further looking to the frequency variable EMSE results shown in Figure 7 (a), it is possible to observe that, as expected, electromagnetic shielding for *Onyx*™ without CF (line with blue dots) increases with the wave frequency. The shielding for *Onyx*™ occurs because the filament is filled with chopped CF which provide some shielding ability to the specimen. However, it remains below 10 dB at the complete frequency range. Furthermore, the collected data for the composite specimens with at least one CF layer showed some resonant characteristics bellow 800 MHz, in contrast to the stable and linear growth seen with *Onyx*™ (0 CF). This effect is still not fully comprehended but it may be originated due to an antenna effect induced by the continuous CF length.

Additionally, the EM wave interaction with specimens with continuous CF layers has a particular effect. It can be noted that, above 1 GHz, the shielding provided from the CF layers decreased with the frequency, as opposed to the effect in specimens made entirely with *Onyx*™. This shielding drop can be reasonably explained by the shorter waves travelling through gaps in the mesh screen created by the stacked CF layers, as can be seen in metallic wire meshes or ventilation panels or scaffolds, where the shielding performance is governed by the cross-section and depth of the apertures [3,15,26]. However, this effect was not expected for wavelength at which this study is done, as the dimension of these gaps or voids are much smaller than half the wavelength.

When analyzing the shielding properties for a given material, it is important to distinguish the discrete mechanisms of absorption (SE_A) (Figure 8 (b)), reflection (SE_R) (Figure 8 (c)), and the total shielding (SE_T), which is the sum of the two components, as mentioned in section *2. Materials and methods*.

Preprints (www.preprints.org) | NOT PEER-REVIEWED | Posted: 12 October 2023 doi:10.20944/preprints202310.0758.v1

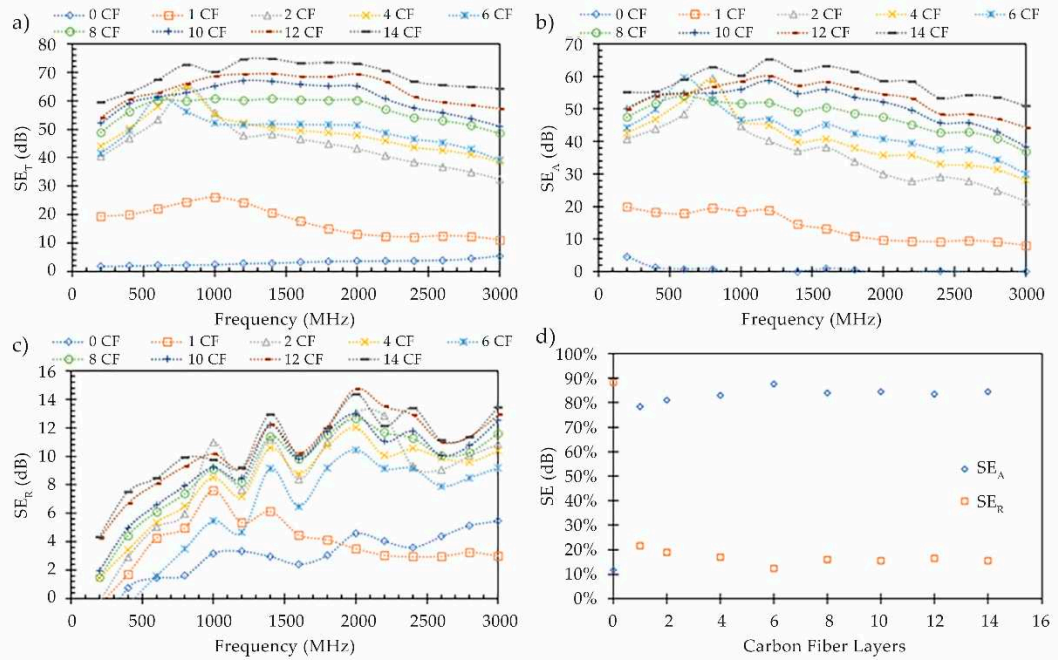

Figure 8. EMSE results: (a) total shielding (SE_T) along the frequency range; (b) absorption shielding (SE_A) along the frequency range; (c) reflection shielding (SE_R) along the frequency range; and (d) average ratio for each shielding mechanism.

This analysis evidence that, with the exception for *Onyx*™ specimen (0 CF), the absorption is the most dominant mechanism of shielding for the printed composite specimens. On average, the absorption of EM waves is responsible for approximately 80% of the shielding behavior. Furthermore, the absorption ratio appears to increase with the increment of the number of CF layers, meaning that this approach of additive manufacturing based in continuous CF deposition can result in rather suitable radar absorber materials.

The main reason for the shielding improvement with the addition of more CF layers is the much higher electrical conductivity of the continuous CF layers relatively to the chopped CF inside the *Onyx*™ baseline material. The electrical resistivity for both *Onyx*™ and CF filaments was measured before and after these materials were subject to the printing process. The electrical resistivity results, shown in Table 4, evidence that CF has as resistivity between 1 to 23 Ω.cm which is almost 10 orders of magnitude lower than the electrical resistivity of *Onyx*™. However, since the printing of continuous CF is restricted to the inner layers of the specimen (*Onyx*™ in printed on the bottom and top layers), the reduction of electrical resistivity with the increase of CF layers was not observed in the experimental measures. All composite specimens exhibited resistivity in the order of 1 x 10^{11} Ω.cm, which is near the values measured for the specimen without continuous CF.

Table 4. Measured electrical resistivity (ρ) for filaments and printed specimens.

Filament	***Onyx*™**		**Carbon fiber**	
	Pre-processing	***Post-processing***	***Pre-processing***	***Post-processing***
ρ(Ω.cm)	2.11 x10^{+10}	8.16 x10^{+9}	1.18	23.32

Specimen	**0 CF**	**1CF**	**2 CF**	**4 CF**	**6 CF**	**8 CF**	**10 CF**	**12 CF**	**14 CF**
ρ(Ω.cm) x10^{+11}	6.59	5.36	5.86	4.81	4.41	4.24	4.16	4.69	1.37

If one tries to derive the EM shielding performance from the electrical resistivity measured at the as-build specimens will figure that, for this type of material, the shielding estimations will be underestimated and will not translate the real measured values and shown in the previous graphs.

Preprints (www.preprints.org) | NOT PEER-REVIEWED | Posted: 12 October 2023 doi:10.20944/preprints202310.0758.v1

As can be seen in Figure 9, if one assumes a resistivity above 10^{11} Ω.cm, as measured, the shielding should be almost zero. But instead, the actual shielding of the specimens is, depending on the amount of CF layers, from 10 up to 70 dB. In order to achieve this level of shielding magnitude the electrical resistivity must be near or below 20 Ω.cm, which corresponds to the resistivity measured for the isolated carbon fibers. Therefore, the CF inherent electrical properties are the ones that should be considered if someone needs to calculate the EM shielding from theoretical models.

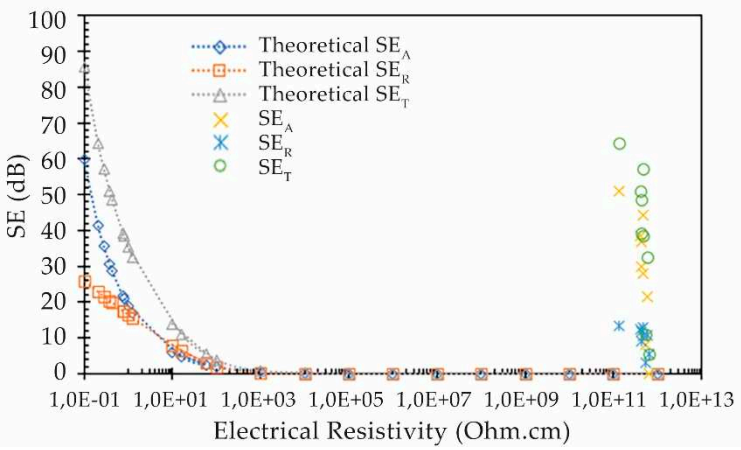

Figure 9. EM shielding and electrical resistivity relation. EMSE is expected to decrease for higher resistivities by power law.

As mentioned, and reported elsewhere [26,42,56], the thickness and density of the parts can influence the composites' EM shielding. Therefore, the normalized shielding (SE divided by the specimen's thickness) and the specific shielding (SE divided by the specimen's density) was calculated and is presented in Figure 10 and Figure 11, respectively.

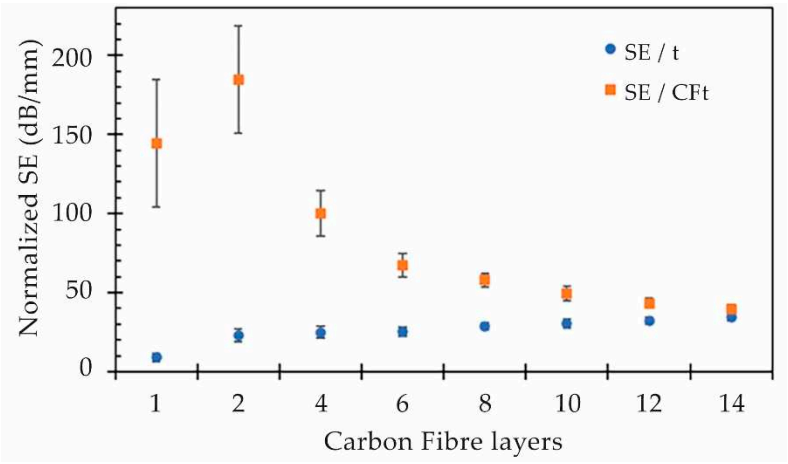

Figure 10. Normalized shielding effectiveness for the specimen's thickness (t) and per added CF layer thickness (CFt).

As one can observe (in the blue circles), the developed composites with at least two CF layers reached a normalized shielding (SE/t) from 23 dB/mm up to 34 dB/mm, depending on the number of CF layers. Where it grows linearly by a factor of 1.2 with the increase two additional CF layers. If these composites were a homogeneous material, one could assume that it's possible to improve the shielding by almost 30 dB per each additional millimeter of thickness added to the part. However, the shielding effect is promoted by the inner CF layers of the total composite thickness. Therefore, one can adjust the normalized shielding taking into consideration the isolated CF layer thickness by dividing the measured EMSE by the effective CF thickness (SE/CFt). The adjusted values (orange squares) reveals that the CF layer can achieve a SE of almost 185 dB/mm for the composite with two

Preprints (www.preprints.org) | NOT PEER-REVIEWED | Posted: 12 October 2023 doi:10.20944/preprints202310.0758.v1

CF layers and for greater amount of CF the shielding effectiveness decays with the increase of two combined CF layers by a power-law function with an average power of -0.7.

Regarding the specific shielding (SE/ϱ), is an important metric to consider when producing lightweight components. A higher specific shielding means that a better EM barrier can be achieved with a lightweight material, which an important aspect for energy savings. One can observe, in the Figure 11, that above two CF layers these composites have a specific shielding from near 40 db.cm³/g up to 60 dB.cm³/g.

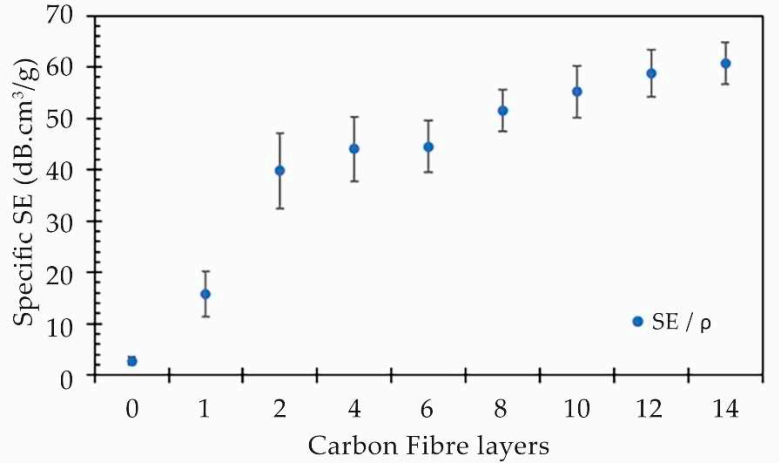

Figure 11. Specific EM Shielding for each composite formulation.

When compared to other composites produced by additive manufacturing, specifically ME technology, it is noticeable that the printed composites with continuous carbon fiber have better performance than materials fabricated by other researchers. The printed composites with at least two CF layers have an average shielding between 45 to 70 dB, normalized shielding between 23 to 34 dB/mm and specific shielding between 40 to 60 dB.cm³/g. Such performance is well above the average shielding of 30 dB, normalized shielding of almost 21 dB/mm and specific shielding of approx. 42 dB.cm³/g obtained in peer studies [26,37,41–43]. However, as previously mentioned, the use of additive manufacturing of continuous CF for electromagnetic shielding applications is a novel work and we were unable to find a direct peer study to compare the results. But one can compare to materials produced by conventional molding technologies, like injection molding [15,27] or compression molding [52,54,57–59], and verified that the developed material has similar or better performance than the other materials.

4. Conclusions

The printing of continuous carbon fiber by material extrusion technique was used to produce 2 mm thick composite parts with electromagnetic shielding that can reach 70 dB in the frequency band of 0.03 – 3 GHz. This is an improvement of more than 22 times, from the baseline printed composite polyamide material (*Onyx*™) without any continuous carbon fiber layer. From a commercial standpoint, a material capable of achieve an electromagnetic shielding above 30 dB, which blocks more than 99.9% of electromagnetic waves from being transmitted is considered adequate for practical applications. Therefore, this research evidence an innovative and customizable approach to produce lightweight enclosures for electromagnetic shielding purposes.

One of the advantages of these composites is related to the possibility to fit the performance as required by easily modifying the internal structure of the composite, since, depending on the carbon fiber layers and the frequency of interest, these composites can reach an electromagnetic shielding efficiency in the range of 40 to 70 dB, or even higher for thicker specimens. The effect of the number of carbon fiber layers was evaluated and it was found that an increase of a combination of two carbon fiber layers lead to a linear increase of shielding at a rate of approx. 4 dB, which corresponds to an effectiveness increase of almost 2 dB/mm. However, above two carbon fiber layers the addition of

carbon fiber tends to be less effective since the electromagnetic shielding efficiency improvement per added carbon fiber layer diminishes following a power-law function with a power of -0.7.

This study also found that the absorption shielding (SEA) for these additive manufacturing composite materials have ranges between 80% to 90%, which thus demonstrates the adsorption-dominated shielding mechanism. This aspect and a specific shielding up to 60 dB.cm^3/g places these additive manufacturing composites as a possible and rather new lightweight solution for electromagnetic shielding, specifically for applications which require a high absorption rate.

Author Contributions: The manuscript was written through contributions of all authors. Martins, L.C.: Methodology, investigation, formal analysis, writing – original draft; Fernandes, L.C.: methodology. Silva, C.S.: writing: review & editing; Sampaio, Á.M.: supervision, writing — review and editing; Pontes, A.J.: supervision, writing: review and editing, Funding acquisition. All authors have read and agreed to the published version of the manuscript.

Funding: This research was co-funded by the European Regional Development Fund through the Operational Competitiveness and Internationalization Programme (COMPETE 2020) [Project No. 47108, "SIFA"; Funding Reference: POCI-01-0247-FEDER-047108] and by the Foundation for Science and Technology (FCT) through the PhD scholarship 2020.04520.BD.

Acknowledgments: The authors would like to acknowledge that the present research was co-funded by the European Regional Development Fund (ERDF) through the Operational Competitiveness and Internationalization Programme (COMPETE 2020) of the Portugal 2020 Program [Project No. 47108, "SIFA"; Funding Reference: POCI-01-0247-FEDER-047108].

Conflicts of Interest: The authors declare no conflict of interest.

References

1. Chikyu, N.; Nakano, T.; Kletetschka, G.; Inoue, Y. Excellent electromagnetic interference shielding characteristics of a unidirectionally oriented thin multiwalled carbon nanotube/polyethylene film. *Materials & Design*. **2020**; *195*, 1-9.
2. Kaiser KL. *Electromagnetic Shielding*, 1st ed.; CRC Press: Boca Raton, USA, 2005.
3. Tong XC. *Advanced Materials and Design for Electromagnetic Interference Shielding*, 1st ed.; CRC Press: Boca Raton, USA, 2009.
4. Chung, D.D.L. Materials for Electromagnetic Interference Shielding. J. *Mater. Eng. Perform.* **2000**; *9*, 350–354.
5. Aciu, L.E.V.; Ogrutan, P.L.P.; Badic, M.V. New Methods Developed for Shielding Materials Characterization. *Ann. Univ. Craiova, Electr. Eng. Ser.* **2009**; 1–4.
6. Geetha, S.; Kumar, K.K.S.; Rao, C.R.K.; Vijayan, M.; Trivedi, D.C. EMI Shielding: Methods and Materials — A Review. *J. Appl. Polym. Sci.* **2009**; 112, 2073–2086.
7. Bryant, N. Using Long Fiber Nickel Coated Carbon Fiber (LFNCCF) to produce Light Weight EMI Shielding Plastic Composites. In: *2013 IEEE International Symposium on Electromagnetic Compatibility*, 1st ed.; IEEE: Denver, CO, USA, 2013, 371–375.
8. Morari, C.; Balan, I.; Pintea, J.; Elena, C.; Iordache, I. Electrical Conductivity and Electromagnetic Shielding Effectiveness of Silicone Rubber Filled with Ferrite and Graphite Powders. *Prog. Electromagn. Res. M.* **2011**, *21*: 93–104.
9. Al-saleh, M.H.; Sundararaj, U. Electromagnetic interference shielding mechanisms of CNT / polymer composites. *Carbon* **2009**, *47*: 1738–1746.
10. Fan, J.; Zhang, L.; Wei, S.; Zhang, Z.; Choi, S.-K.; Song, B.; Shi, Y. A review of additive manufacturing of metamaterials and developing trends. *Materials Today* **2021**, *50*, 303-328
11. Yuan, S.; Li, S.; Zhu, J.; Tang, W. Additive manufacturing of polymeric composites from material processing to structural design. *Compos. Part B: Eng.* **2021**, 219, 1-25.
12. Saini, P.; Arora, M. Microwave Absorption and EMI Shielding Behavior of Nanocomposites Based on Intrinsically Conducting Polymers, Graphene and Carbon Nanotubes. In: *New Polymers for special applications*, 1st ed.; Gomes, A.D.S., Eds; IntechOpen. Croatia, 2012, 71–112.
13. Jiang, D.; Murugadoss, V.; Wang, Y.; Lin, J.; Ding, T.; Wang, Z.; Shao, Q.; Whang, C.; Liu, H.; Wei, R.; Subramania, A.; Guo, Z. Electromagnetic Interference Shielding Polymers and Nanocomposites - A Review. *Polymer Reviews*, **2019**, *59*, 280–337.
14. Das, T.K.; Prusty, S. Review on Conducting Polymers and Their Applications. *Polym. – Plast. Technol. Eng.*, **2012**, *51*, 1487–1500.
15. Martins, L.C.; Pontes, A.J. Fiber reinforced thermoplastics compounds for electromagnetic interference shielding applications. *J. Reinf. Plast. Compos.*, **2021**, *41*, 206-214.

16. Chiu, S.K.; Cheng, J.Y.; Jou, W.S.; Jong, G.-J.; Wang, S.C.; Wang, C.M.; Lin, C.S.; Wu, T.L.; Cheng, W.H. Electromagnetic shielding of plastic material in laser diode modules. In: *IEEE Electronic Components and Technology Conference Proceedings*. 2001, 645–647.
17. Thomassin, J.M.; Jérôme, C.; Pardoen, T.; Bailly, C.; Huynen, I.; Detrembleur, C. Polymer/carbon based composites as electromagnetic interference (EMI) shielding materials. *Mater. Sci. Eng. R. Reports,* **2013**, *74*, 211–232.
18. Chung, D.D. Electromagnetic interference shielding effectiveness of carbon materials. *Carbon*, **2001**, *39*, 279–285.
19. Sankaran, S.; Deshmukh, K.; Ahamed, M.B.; Pasha, S.K.K. Recent advances in electromagnetic interference shielding properties of metal and carbon filler reinforced flexible polymer composites: A review. *Compos. Part A: Appl. Sci. Manuf.*, **2018**, *114*, 49–71.
20. Al-Saleh, M.H.; Sundararaj, U. Electromagnetic interference (EMI) shielding effectiveness of PP/PS polymer blends containing high structure carbon black. *Macromol. Mater. Eng.* **2008**, *293*, 621–630.
21. Ameli, A.; Jung, P.U.; Park, C.B. Low Percolation Threshold and Improved Electromagnetic Interference Shielding Effectiveness Polypropylene/Carbon Fiber Composites Through Foaming. In: *SPE-ANTEC Proceedings*, **2013**, 6–11.
22. Mahmoodi, M.; Arjmand, M.; Sundararaj, U.; Park, S. The electrical conductivity and electromagnetic interference shielding of injection molded multi-walled carbon nanotube/polystyrene composites. *Carbon* **2012**, *50*, 1455–1464.
23. Arjmand, M.; Mahmoodi, M.; Gelves, G.A.; Park, S.; Sundararaj, U. Electrical and electromagnetic interference shielding properties of flow-induced oriented carbon nanotubes in polycarbonate. *Carbon* **2011**, *49*, 3430–3440.
24. Arjmand, M.; Apperley, T.; Okoniewski, M.; Sundararaj, U. Comparative study of electromagnetic interference shielding properties of injection molded versus compression molded multi-walled carbon nanotube/polystyrene composites. *Carbon* **2012**, *50*, 5126–5134.
25. Al-saleh, M.H.; Sundararaj, U. Microstructure, Electrical, and Electromagnetic Interference Shielding Properties of Carbon Nanotube/Acrylonitrile – Butadiene – Styrene Nanocomposites. *J.Polym. Sci. - Part B Polym. Phys.* **2012**, *50*, 1356–1362.
26. Chizari, K.; Arjmand, M.; Liu, Z.; Sundararaj, U.; Therriault, D. Three-dimensional printing of highly conductive polymer nanocomposites for EMI shielding applications. *Mater. Today Commun.* **2017**, *11*, 112–118.
27. Martins, L.C.; Barbosa, C.N.; Silva, S.; Bernardo, P.; Dias, G.R.; Pontes, A.J. Effect of processing conditions on electromagnetic shielding and electrical resistivity of injection-molded polybutylene terephthalate compounds. *Polym. Eng. Sci.* **2021**, *6*, 2576–2588.
28. Wang, G.; Zhao, G.; Wang, S.; Zhang, L.; Park, C.B. Injection-molded microcellular PLA/graphite nanocomposites with dramatically enhanced mechanical and electrical properties for ultra-efficient EMI shielding applications. *J. Mater. Chem. C* **2018**, 6, 6847–6859.
29. Zhang, Y.; Wang, Z.; Zhang, Y.; Gomes, S.; Bernard, A. Bio-inspired generative design for support structure generation and optimization in Additive Manufacturing (AM). *CIRP Ann.* **2020**, *69*, 117–120.
30. Hoang, V.N.; Nguyen, N.L.; Tran, P.; Qjan, M.; Nguyen-Xuan, J. Adaptive Concurrent Topology Optimization of Cellular Composites for Additive Manufacturing. *JOM* **2020**, *72*, 2378–2390.
31. Nath, S.D.; Nilufar, S. An overview of additive manufacturing of polymers and associated composites. *Polymers* **2020**, *12*, 1–33.
32. Redwood, B.; Schöffer, F.; Garret, B. *The 3D Printing Handbook: Technologies, design and applications*, 1st ed.; 3D Hubs: Amsterdam, Netherlands, 2017, pp. X-X.
33. Ngo, T.D.; Kashani, A.; Imbalzano, G.; Nguyen, K.T.Q.; Hui, D. Additive manufacturing (3D printing): A review of materials, methods, applications and challenges. *Compos. Part B: Eng.* **2018**, *143*, 172–196.
34. Motaparti, K.P. Effect of Build Parameters on Mechanical Properties of Ultem 9085 Parts By Fused Deposition Modeling. Master Theses, Missouri University of Science and Technology, Missouri, 2016.
35. Ferreira, R.T.L; Amatte, I.C.; Dutra, T.A.; Bürger, D. Experimental characterization and micrography of 3D printed PLA and PLA reinforced with short carbon fibers. *Compos. Part. B: Eng.* **2017**, *124*, 88–100.
36. Dorigato, A.; Moretti, V.; Dul, S.; Unterberger, S.H.; Pegoretti, A. Electrically conductive nanocomposites for fused deposition modelling. *Synth. Met.* **2017**, *226*, 7–14.
37. Schmitz, D.P.; Ecco, L.G.; Dul, S.; Pereira, E.C.L.; Soares, B.G.; Barra, G.M.O.; Pegoretti, A. Electromagnetic interference shielding effectiveness of ABS carbon-based composites manufactured via fused deposition modelling. *Mater. Today Commun.* **2018**, *15*, 70–80.
38. Mohan, V.B.; Krebs, B.J.; Bhattacharyya D. Development of novel highly conductive 3D printable hybrid polymer-graphene composites. *Mater. Today Commun.* **2018**, *17*, 554–561.
39. Li. Y.; Feng, Z.; Huang, L.; Essa, K.; Bilotti, E.; Zhang, H.; Peijs, T.; Hao, L. Additive manufacturing high performance graphene-based composites: A review. *Compos. Part A: Appl. Sci. Manuf.* **2019**, *124*, 105483.

40. Hohimer, C.J.; Petrossian, G.; Ameli, A.; Mo, C.; Pötschke, P. 3D printed conductive thermoplastic polyurethane/carbon nanotube composites for capacitive and piezoresistive sensing in soft pneumatic actuators. *Addit. Manuf.* **2020**, *34*, 101281.
41. Schmitz, D.P.; Dul, S.; Ramoa, S.D.A.S.; Soares, B.G.; Barra, G.M.O.; Pegoretti, A. Effect of printing parameters on the electromagnetic shielding efficiency of ABS/carbonaceous-filler composites manufactured via filament fused fabrication. *J. Manuf. Process* **2021**, *65*, 12–19.
42. Lee, K.P.M.; Baum, T.; Shanks, R.; Daver, F. Electromagnetic interference shielding of 3D-printed graphene–polyamide-6 composites with 3D-printed morphology. *Addit. Manuf.* **2021**, *43*, 102020.
43. Wang, Y., Fan, Z.W.; Zhang, H.; Guo, J.; Yan, D.-X.; Wang, S.; Dai, K.; Li; Z.-M. 3D-printing of segregated carbon nanotube/polylactic acid composite with enhanced electromagnetic interference shielding and mechanical performance. *Mater. & Des.* **2021**, *197*, 109222.
44. Duan, Y.; Liang, Q.; Yang, Z.; Li, Z.; Yin, H.; Cao, Y.; Li, D. A wide-angle broadband electromagnetic absorbing metastructure using 3D printing technology. *Mater. & Des.* **2021**, *208*, 109900.
45. Parmiggiani, A.; Prato, M.; Pizzorni, M. Effect of the fiber orientation on the tensile and flexural behavior of continuous carbon fiber composites made via fused filament fabrication. *The Int. J. Adv. Manuf. Technol.* **2021**, *114*, 2085–2101.
46. Blok, L.G.; Longana, M.L.; Yu, H.; Woods, B.K.S. An investigation into 3D printing of fibre reinforced thermoplastic composites. *Addit. Manuf.* **2018**, *22*, 176–186.
47. Markforged Material Datasheet Composites 2022, 2. Available online: https://www-objects.markforged.com/craft/materials/CompositesV5.2.pdf (accessed on 30 September 2023).
48. ASTM International. ASTM D 4935-99: Standard Test Method for Measuring the Electromagnetic Shielding Effectiveness of Planar Materials. 1999; 10.02: 10.
49. Hong, Y.K.; Lee, C.Y.; Jeong, C.K.; Lee, D.E.; Kim, K.; Joo, J. Method and apparatus to measure electromagnetic interference shielding efficiency and its shielding characteristics in broadband frequency ranges. *Rev. Sci. Instrum.* **2003**, *74*, 1098–1102.
50. Sarto, M.S.; Tamburrano, A. Innovative test method for the shielding effectiveness measurement of conductive thin films in a wide frequency range. IEEE *Trans. Electromagn. Compat.* **2006**, *48*, 331–341.
51. Vasquez, H.; Espinoza, L.; Lozano, K.; Foltz, H.; Yang, S. Simple Device for Electromagnetic Interference Shielding Effectiveness Measurement. *IEEE Trans. Electromagn. Compat.* **2009**, 62–68.
52. Andersen, P. International electrotechnical commission documents CISPR 12 and CISPR 25 - An overview. *IEEE Int. Symp. Electromagn. Compat.* 2007, 1-4.
53. Oliveira, F.M.; Martins, L.; Dencheva, N.V.; Ezquerra, T.A.; Denched, Z.Z. Tunable Electromagnetic Interference Shielding Properties of Binary Thermoplastic Composites Prepared by Reactive Microencapsulation. *ACS Appl. Polym. Mater.* **2022**, *4*, 3482–3490.
54. Ren. F.; Li, Z.; Xu, L.; Sun, Z.; Ren, P.; Yan, D.; Li, Z. Large-scale preparation of segregated PLA/carbon nanotube composite with high efficient electromagnetic interference shielding and favourable mechanical properties. *Compos. Part B: Eng.* **2018**, *155*, 405–413.
55. Kong, W.; Yi, S.; Sun, W.; Xu, L.; Jia, L.; Yan, D.; Li, Z. Polyaniline-decorated carbon fibers for enhanced mechanical and electromagnetic interference shielding performances of epoxy composites. *Mater. & Des*, **2022**, *217*, 110658.
56. Cui, C.H.; Yan, D.X.; Pang, H.; Jia, L.-C.; Xu, X.; Yang, S.; Xu, J.Z., Li, Z.-M. A high heat-resistance bioplastic foam with efficient electromagnetic interference shielding. *Chem. Eng. J.* **2017**, *323*, 29–36.
57. Song, P.; Liang, C.; Wang, L.; Qiu, H.; Gu, H.; Kong, J.; Gu, J. Obviously improved electromagnetic interference shielding performances for epoxy composites via constructing honeycomb structural reduced graphene oxide. *Compos. Sci. Technol.* **2019**, *181*, 107698.
58. Kashi, S.; Gupta, R.K.; Baum, T.; Kao, N.; Bhattacharya, S.N. Morphology, electromagnetic properties and electromagnetic interference shielding performance of poly lactide/graphene nanoplatelet nanocomposites. *Mater. & Des.* **2016**, *95*, 119–126.
59. Gedler, G.; Antunes, M.; Velasco, J.I.; Ozisik, R. Enhanced electromagnetic interference shielding effectiveness of polycarbonate/graphene nanocomposites foamed via 1-step supercritical carbon dioxide process. *Mater. & Des.* **2016**, *90*, 906–914.